

BoxVIS: Video Instance Segmentation with Box Annotations

Minghan Li and Lei Zhang*

Department of Computing, Hong Kong Polytechnic University

liminghan0330@gmail.com, cslzhang@comp.polyu.edu.hk

Abstract

It is expensive and labour-extensive to label the pixel-wise object masks in a video. As a results, the amount of pixel-wise annotations in existing video instance segmentation (VIS) datasets is small, limiting the generalization capability of trained VIS models. An alternative but much cheaper solution is to use bounding boxes to label instances in videos. Inspired by the recent success of box-supervised image instance segmentation, we first adapt the state-of-the-art pixel-supervised VIS models to a box-supervised VIS (BoxVIS) baseline, and observe only slight performance degradation. We consequently propose to improve BoxVIS performance from two aspects. First, we propose a box-center guided spatial-temporal pairwise affinity (STPA) loss to predict instance masks for better spatial and temporal consistency. Second, we collect a larger scale box-annotated VIS dataset (BVISD) by consolidating the videos from current VIS benchmarks and converting images from the COCO dataset to short pseudo video clips. With the proposed BVISD and the STPA loss, our trained BoxVIS model demonstrates promising instance mask prediction performance. Specifically, it achieves 43.2% and 29.0% mask AP on the YouTube-VIS 2021 and OVIS valid sets, respectively, exhibiting comparable or even better generalization performance than state-of-the-art pixel-supervised VIS models by using only 16% annotation time and cost. Codes and data of BoxVIS can be found at <https://github.com/MinghanLi/BoxVIS>.

1. Introduction

Video instance segmentation (VIS) aims to predict the pixel-wise masks and categories of instances over the input video. The recently proposed VIS methods [14–16, 36–38] have achieved much progresses on the YouTube-VIS [41] and OVIS [29] benchmark datasets. Generally speaking, these methods first partition the whole video into individual frames or short clips to extract per-frame or per-clip features

Methods	Superv.	Annot.	YTVIS21	OVIS
M2F-VIS	Pixel	485d	43.2	24.5
M2F-VIS-box	Box	43d	41.2 ^{-2.0}	23.9 ^{-0.6}
BoxVIS (ours)	Box	80d	43.2 ^{+0.0}	29.0 ^{+4.5}

Table 1. Performance (Mask AP) comparison of pixel-supervised Mask2Former-VIS (M2F-VIS) [7], its box-supervised VIS (BoxVIS) counterpart M2F-VIS-box, and our BoxVIS method on YTVIS21 and OVIS valid sets.

and predict instance masks, and then associate the predicted masks across frames/clips based on the embedding similarity of instances. However, all the current VIS methods require pixel-wise annotations, where the pixels belonging to the target instances are labeled as 1 and others as 0, to train the VIS model for pixel-wise mask prediction.

Compared with image instance segmentation (IIS), VIS requires a larger number of annotated training data due to the existence of object motion and complex trajectories in videos. Unfortunately, it is an expensive and labour-extensive task to label the pixel-wise object masks in a video. As a result, the amount of pixel-wise annotations in existing VIS datasets is small. For example, there are only 8k and 5k labeled instances in YouTube-VIS 2021 (YTVIS21) and OVIS, respectively, which limits the generalization capabilities of trained VIS models. However, it has been demonstrated [24, 28] that labeling the bounding box of an object takes only 8.8% (7s vs. 79.2s) the time of labeling its polygon-based mask in COCO [24]. Actually, a few box-supervised IIS methods [9, 19, 20, 22, 31] have been recently developed and achieved competitive performance with pixel-supervised IIS methods. Therefore, one natural and interesting question is: can we use bounding boxes to label instances to train the VIS models?

To validate the feasibility of VIS with only box annotations, we adapt the state-of-the-art pixel-supervised VIS models to a box-supervised VIS (BoxVIS) baseline. Specifically, inspired by the box-supervised IIS methods BoxInst [31] and BoxTeacher [9], we introduce two box-supervised segmentation loss terms, the projection loss and the pairwise affinity loss, into the pixel-supervised VIS method Mask2Former-VIS (M2F-VIS) [7], and replace the ground-

*Corresponding author.

truth masks with the produced pseudo masks to supervise the model learning. (Please refer to Section 3.1 for details.) Denote by M2F-VIS-box the adapted BoxVIS model from M2F-VIS. As shown in Table 1, compared with M2F-VIS, M2F-VIS-box drops only 2.0% and 0.6% mask AP on YTVIS21 and OVIS valid sets, respectively. We think there are two main reasons for the slight performance degradation. First, all current VIS models have been pre-trained on the COCO dataset before fine-tuned on the VIS datasets. There is a large overlap of categories between the COCO and VIS datasets so that the pre-training enables a good baseline VIS model. Second, when fine-tuning on videos, ground-truth boxes and pseudo masks actually provide comparable supervision to pixel-wise annotation to learn object motion and appearance changes.

Nonetheless, there are two challenging issues for BoxVIS. First, without pixel-wise labeling, the box-level annotation cannot explicitly tell the segmenter the precise boundary and the temporal association of objects. It is essential to investigate how to make the VIS models have good object spatial-temporal consistency with only box annotations. Second, objects in videos often have significant position shifts, appearance changes, heavy occlusion, uncommon camera-to-object views, *etc*. To deal with the diverse variations of videos, a larger scale box-annotated dataset is required to train robust BoxVIS models.

With the above considerations, we propose to improve the BoxVIS performance from two aspects: modeling the object spatial-temporal consistency and increasing the amount of box-annotated video clips. First, we propose a box-center guided spatial-temporal pairwise affinity (STPA) loss to predict instance masks with better spatial and temporal consistency. Second, we collect a larger box-annotated VIS dataset (BVISD) by consolidating the videos from current VIS benchmarks and converting some images from COCO to short pseudo video clips. The trained BoxVIS model with the proposed STPA loss and BVISD demonstrates promising instance segmentation results, achieving 43.2% and 29.0% mask AP on YouTube-VIS 2021 and OVIS valid sets, respectively. It obtains comparable or even better generalization performance than the pixel-supervised VIS competitors by using only 16% annotation time and cost, exhibiting great potentials.

2. Related Work

2.1. Pixel-supervised VIS

There are two major VIS benchmarks, the YTVIS series [41] and OVIS [29], which have very different video types in terms of object motions and scenes. The YTVIS series focus mainly on segmenting sparse objects in shorter videos, while the OVIS aims to segment crowded instances with occlusions in longer videos. Based on these facts, we

categorize the pixel-supervised VIS models into YTVIS-oriented ones and OVIS-oriented ones.

YTVIS-oriented VIS models. By introducing a tracker into the representative IIS methods [3, 13, 30], the early proposed VIS methods [1, 4, 12, 17, 21, 25, 41, 42] have achieved decent performance on YTVIS series. The frame-to-frame trackers [4, 12, 21, 41] integrate the clues such as category score, box/mask IoU and instance embedding similarity. The clip-to-clip trackers [1, 2, 16, 21, 23, 29, 36, 37] propagate the predicted instance masks from a key frame to other frames, which can be implemented by deformable convolution [2, 10], non-local block [23], correlation [21, 29], graph neural network [33], *etc*.

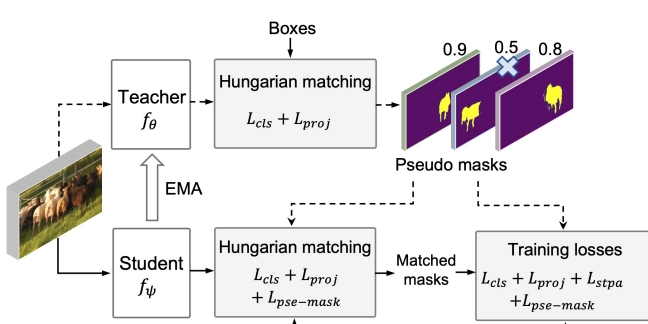
Recently, query-based [5] VIS methods [16, 36, 37, 39] have achieved impressive progress. VisTR [36] views the VIS task as an end-to-end parallel sequence prediction problem, but it consumes a large amounts of memory to store spatial-temporal features. To solve the issue, IFC [16] transfers inter-frame information via efficient memory tokens, and SeqFormer [37] locates an instance in each frame and aggregates them to predict video-level instances.

OVIS-oriented VIS models. The above mentioned YTVIS-oriented VIS models often fail to handle the challenging long videos with crowded and similar-looking objects in OVIS dataset, resulting in significant performance degradation. Inspired by contrastive learning [6, 18, 27, 35], IDOL [38] learns discriminative embeddings for multiple object tracking frame by frame. Masked-attention transformer [8] brings significant performance improvement on OVIS dataset by calculating attention only in the region of the objects. Mask2Former-VIS [7] with per-clip input takes the mask IoU of the overlapping frames as the tracker, while MinVIS [15] with per-frame input employs instance embedding similarity by using Hungarian matching as the tracker. VITA [14] integrates the predicted object embeddings of all frames in the video to produce video-level instance masks.

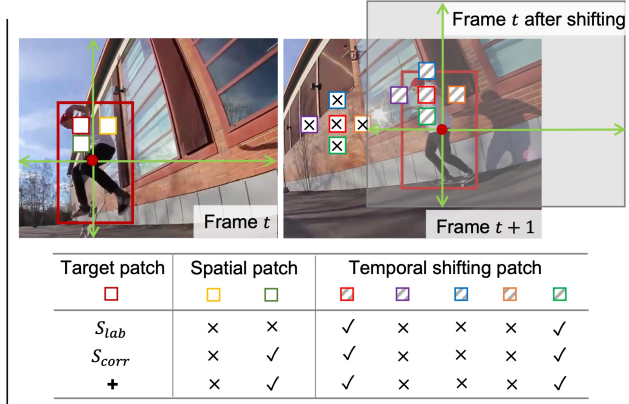
Remarks. Though the pixel-supervised VIS methods have achieved much progress, their generalization capability is limited. For example, the VIS models trained on YTVIS21 often fail to handle the challenging videos in OVIS, due to the limited number of type of videos in each dataset. However, it is labour-extensive to label the pixel-wise masks in videos. Inspired by the success of box-supervised IIS methods, we explore video instance segmentation with only box annotations in this paper.

2.2. Box-supervised IIS

A few box-supervised IIS methods have been proposed. BoxCaseg [34] leverages a salience model to generate pseudo object masks to train a Mask R-CNN along with the multiple instance learning (MIL) loss. Recently, BoxInst [31] achieves impressive performance by proposing a projection loss and a pairwise affinity loss for box-supervision.



(a) Overview of our BoxVIS architecture



(b) Box-center guided spatial-temporal pairwise affinity (STPA) Loss

Figure 1. (a) Architecture of our proposed BoxVIS, where the Teacher and Student Nets follow the Mask2Former-VIS [7] framework. The Teacher Net produces high-quality object masks, which are assigned as the pseudo instance masks of the ground-truth bounding boxes by Hungarian matching. The predicted masks from the Student Net will be matched with the ground-truth boxes and the generated pseudo masks by taking the assigned pseudo masks into account. (b) Schematic diagram of the proposed spatial-temporal pairwise affinity (STPA) loss, which uses box-center guided shifting to generate temporally paired pixels and employs the color similarity S_{lab} and patch correlation S_{corr} to compute pairwise affinity.

BoxLevelSet [22] utilizes the traditional level set evolution to predict the object boundaries and instance masks. DiscoBox [20] and BoxTeacher [9] employ an exponential moving average teacher to produce high-quality pseudo instance masks and introduce pseudo pixel-wise mask supervision, bringing significant performance improvement. In this work, we propose the first box-supervised VIS framework and demonstrate its effectiveness.

3. Methodology

We first extend the pixel-supervised VIS methods to a box-supervised VIS (BoxVIS) baseline in Sec. 3.1, then propose a box-center guided spatial-temporal pairwise affinity loss and a large scale box-annotated VIS dataset (BVISD) in Sec. 3.2 and Sec. 3.3, respectively.

3.1. A BoxVIS Baseline

In this subsection, we first introduce the two box-supervised instance segmentation loss items [31] and the pseudo mask supervision loss with the high-quality pseudo masks generated by exponential moving average teacher [9, 20], then extend the per-clip input based Mask2Former-VIS model [7] to its box-supervised counterpart, namely M2F-VIS-box, as a BoxVIS baseline.

Projection loss [31] supervises the horizontal and vertical projections of the predicted mask using the ground-truth box annotation, which ensures that the tightest box covering the predicted mask matches the ground-truth box. The projection loss is formulated as:

$$L_{proj} = L\left(\max_y(M), \max_y(\bar{B})\right) + L\left(\max_x(M), \max_x(\bar{B})\right),$$

where M indicates the predicted mask, and \bar{B} denotes the ground-truth box mask, where points in the inner bounding box are 1, and otherwise 0.

Pairwise affinity loss [31] is designed to supervise pixel-wise mask prediction without pixel-wise annotation. If two adjacent pixels have similar colors, they are very likely to have the same mask labels. For two pixels located at (x_i, y_i) and (x_j, y_j) , their color similarity is defined as $S_{lab} = \exp(-\frac{\|c_i - c_j\|}{\theta})$, where c_i and c_j are the color vectors in the LAB color space, and θ is a hyper-parameter (set as 2 by default). If the color similarity of two pixels is greater than a threshold τ , they are assumed to have same mask labels, *i.e.*, the edge weight of the two pixels is set to 1. Hence, the pairwise mask affinity is formulated as $P(y_e = 1) = M_i \cdot M_j + (1 - M_i) \cdot (1 - M_j)$, where M_i and M_j represent the predicted masks of the two pixels, respectively. The pairwise affinity loss is formulated as:

$$L_{pair} = -\frac{1}{N} \sum_{e \in E_{in}} \mathbb{1}_{\{S_{lab} \geq \tau\}} \log P(y_e = 1). \quad (1)$$

where E_{in} indicates the set of paired pixels in the inner bounding box, and N is the total number of the pixel pairs with the same labels in E_{in} .

Pseudo mask supervision loss. Exponential moving average (EMA) teacher [9, 20] can generate high-quality instance masks as the pseudo masks of the ground-truth boxes. By replacing the ground-truth masks with the pseudo masks, the pixel-wise mask supervision loss in the pixel-supervised VIS methods can be extended to the pseudo mask supervision loss, termed as $L_{pse-mask}$, which usually consists of the binary cross-entropy loss and the Dice loss

[11,26]. The box-supervised IIS models with EMA employ a sophisticated Teacher Net and a Student Net in training. The Student Net is normally optimized with the aforementioned box-supervised losses and pseudo-mask loss, and the Teacher Net is progressively updated via EMA without back-propagating gradients.

BoxVIS baseline. By using the above two box-supervised loss terms and the pseudo mask supervision loss, we extend the pixel-supervised VIS method Mask2Former-VIS (M2F-VIS) [7] to a BoxVIS baseline, namely M2F-VIS-box. The overall architecture of the BoxVIS baseline is shown in Fig. 1(a). It is composed of a sophisticated Teacher Net f_θ and a Student Net f_ϕ . During training, a short video clip will be fed to the Teacher Net f_θ and Student Net f_ϕ to predict object masks. The predicted masks from the teacher net will be taken as the pseudo masks of the ground-truth boxes by the Hungarian matching algorithm, whose cost matrix consists of the classification loss and the projection loss. On the other hand, the predicted masks from the student net will be matched with the ground-truth boxes and the generated pseudo masks, whose matching cost matrix takes the assigned pseudo masks into account. After that, the matched masks are supervised by the ground-truth boxes and pseudo masks via the aforementioned box-supervised loss and pseudo-mask loss respectively. Finally, the teacher is progressively updated via EMA. During inference, the teacher net will be discarded, and we only use the predicted masks from the student net.

Beside, the low-quality pseudo masks may introduce some incorrect pixel-wise supervision for the pseudo-mask loss, resulting in performance degradation. The confidence scores for estimating the mask quality are computed as the product of the classification score and the projection score. Hence, to select the high-quality pseudo masks, we adopt a dynamic threshold, which is determined by the ratio of the number of processed iterations to the total number of training iterations: $\epsilon = 1/(1+e^{-2(1-r)})$, $r = \text{iters}/\text{total iters}$.

3.2. Spatial-temporal Pairwise Affinity Loss

Segmenting instances from videos is more challenging than segmenting objects from individual images, as videos often have unexpected motion blur, uncommon-camera-to-object, appearance changes, heavy occlusion and so on. The pairwise affinity loss in Eq. (1) only considers the paired pixels within a single frame, which may however fail for BoxVIS to constrain the temporal consistency of segmented objects. One naive solution is to directly select the neighbours at the same positions in the next frame to perform temporal pairwise affinity loss. Unfortunately, objects in a video often change their positions due to camera jitters or object motion. The assumptions that two adjacent pixels in an image will have similar colors and hence the same mask labels do not hold well for adjacent frames in a video. Two

pixels from two adjacent frames may have similar colors but they can belong to different instances. To solve this issue, we propose a box-center guided spatial-temporal pairwise affinity (STPA) loss, which uses the box-center guided shifting to generate the temporally paired pixels, and uses the color similarity and patch correlation in feature space to stably compute the pairwise affinity.

Spatial-temporally paired pixels. For a pixel in a video clip, we only consider its two spatial neighbours in the current frame for efficiency: the right and bottom pixels, named the set E_s of spatial neighbours. We then discuss how to use the bounding box centers to identify inter-frame paired pixels. The object bounding boxes in consecutive frames can indicate coarse inter-frame movements of the objects. For a given instance appeared in two adjacent frames t_i and t_j , we denote by (t_i, x_i^c, y_i^c) and (t_j, x_j^c, y_j^c) its bounding box centers, and by $(dx^c, dy^c) = (x_i^c - x_j^c, y_i^c - y_j^c)$ the location offsets of the two centers. Then, for any pixel at position (t_i, x_i, y_i) in frame t_i , if it locates in the inner bounding box of the instance, we can shift its position to the nearby area of the instance bounding box in frame t_j by $(t_j, x_i + dx^c, y_i + dy^c)$. Consequently, the set E_t of temporal neighbours can be produced by shifting the center pixel and its four spatial neighbours in frame t_i to the corresponding positions in frame t_j . Overall, for each pixel, we group its seven neighbours as paired pixels to compute the proposed STPA loss. The schematic and the generated spatial-temporal pixels are illustrated in Fig. 1(b).

Patch correlation. It is not reliable enough to utilize pixel-to-pixel color similarity to determine whether two pixels have the same labels or not. Therefore, we introduce an extra patch correlation in the feature space to compute stable and reliable temporal pairwise affinity. For a pixel at position (t_i, x_i, y_i) , we represent the pixels in its centered patch as $(t_i, x_i + o_x, y_i + o_y)$, where the displacements $(o_x, o_y) \in [-k, k] \times [-k, k]$ and k controls the patch size (set as 1 by default). The feature correlation of two patches is defined as

$$S_{corr} = \frac{1}{|\Omega|} \sum_{o \in \Omega} \frac{\langle f_{i+o}, f_{j+o} \rangle}{\| f_{i+o} \| \cdot \| f_{j+o} \|}, \quad (2)$$

where f_{i+o} and f_{j+o} are the feature vectors at positions $(t_i, x_i + o_x, y_i + o_y)$ and $(t_j, x_j + o_x, y_j + o_y)$ in the last pixel encoder layer of Mask2Former framework. $|\Omega|$ is the total number of pixels within the patch $\Omega = [-k, k] \times [-k, k]$.

The overall pairwise affinity is $S_e = S_{lab} + 0.5S_{corr}$. To remove the paired pixels with low affinity, we introduce a color similarity threshold τ_{lab} and a correlation threshold τ_{corr} , respectively. The affinity threshold used in our paper is $\tau = \tau_{lab} + 0.5\tau_{corr}$. Without otherwise specified, we set $\tau_{lab} = 0.3$ and $\tau_{corr} = 0.9$ by default, *i.e.*, $\tau = 0.75$. We still adopt the mask pairwise affinity $P(y_e = 1) = M_i \cdot M_j + (1 - M_i) \cdot (1 - M_j)$, and M_i and M_j are the predicted

Datasets	YTVIS21	OVIS	COCO	BVISD
Videos	2985	901	-	3886
Frames	90k	42k	90k	222k
Instances	8k	5k	450k	463k
Objects	232k	296k	450k	978k
Categories	40	25	80	40
Pixel annot.	213d	272d	413d	898d
Box annot.	19d	24d	37d	80d
OL cate.	39	25	25	40

Table 2. Statistics. ‘OL cate.’ refers to the number of overlapping categories with BVISD.

masks at positions (t_i, x_i, y_i) and (t_j, x_j, y_j) , respectively. Finally, the STPA loss can be formulated as:

$$L_{stpa} = -\frac{1}{N} \sum_{e \in E_{stin}} \mathbf{1}_{\{S_e \geq \tau\}} \log P(y_e = 1). \quad (3)$$

where E_{stin} indicates the set of the spatial-temporally paired pixels, among which at least one pixel locates in the inner bounding box of the instance in current frame. N is the total number of the paired pixels with affinity higher than the threshold S_e in the set $E_{stin} = E_s \cup E_t$.

3.3. Box-annotated VIS dataset (BVISD)

It is very costly to annotate fine-grained masks for instances in videos. We propose a larger scale box-annotated VIS dataset (BVISD) by merging the videos from current VIS benchmarks, YouTube-VIS and OVIS, and converting images from the COCO dataset to short pseudo video clips. For YouTube-VIS benchmark, we adopt the latest YTVIS21, which contains 2,985 training videos over 40 categories, and the video length is less than 36 frames. OVIS [29] includes 607 training videos over 25 object categories, but each frame has more objects than YTVIS21 with different occlusion levels.

There are 25 overlapping categories between COCO and VIS benchmarks, including around 90k images and 450k objects. To augment the single image from COCO to a video clip, we first resize the image by adjusting its short edge in the range of [600, 800], and then randomly crop a region with the short edge within [320, 512]. Finally, the cropped region will be randomly rotated with the degree of [-15, 15]. We repeat the above augmentation process for T times to obtain a pseudo video clip with T frames. During training, the short video clip augmented from COCO will be further resized into the input resolution, *i.e.* 360p.

One key step to consolidate the above three datasets is how to properly merge the object categories to avoid semantic conflicts. Fortunately, the 25 categories of OVIS are mostly contained in the 40 categories of YTVIS21, except for the ‘sheep’ category. Besides, the categories ‘car’ and ‘truck’ in YTVIS21 are merged into a super-category ‘ve-

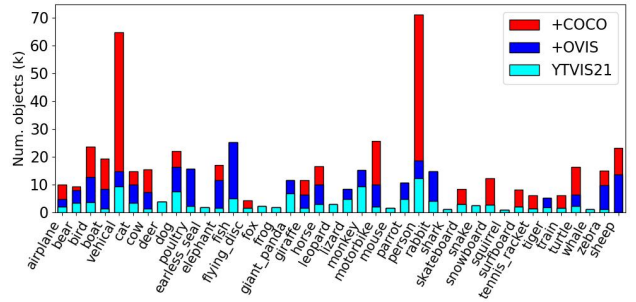


Figure 2. Number of objects per category in BVISD. The number of ‘person’ category is divided by 5 for display.

hicle’ in OVIS. In BVISD, we first merge the similar categories as its super-category to avoid ambiguity, and keep the remaining object categories in YTVIS21 and OVIS. For COCO, we use images that contain at least one object in the categories of BVISD. The distribution of the objects in BVISD is illustrated in Fig. 2.

The statistics of YTVIS21, OVIS, COCO and BVISD are shown in Table 2. Overall, the proposed BVISD consists of 222k frames, 978k objects and 40 non-conflicting object categories. Note that only object box annotations are provided in BVISD. It has been shown [24, 28] that labeling the bounding box of an object takes only 7 seconds, while labeling its polygon-based mask needs 79.2 second in COCO [24]. One can then estimate that annotating the object bounding boxes in BVISD takes $7 \times 978,000$ seconds, about 80 worker days, while labeling the pixel-wise annotations takes $79.2 \times 978,000$ seconds, about 898 worker days.

For easier to test the models, we split the BVISD data into two separated parts: the training set and the valid set, while the valid set contains around 1/10 the videos of BVISD. As shown in Fig. 2, some categories are only presented in YTVIS21 but not OVIS and COCO, which may result in unbalanced categories. During training, therefore, we sample the clips from the three datasets with different sampling weights to alleviate the issue. During inference, we test our proposed BoxVIS in the three valid sets: official YTVIS21 valid, official OVIS valid and our BVISD valid. For the testing on official YTVIS21 and OVIS valid sets, the predicted categories will be mapped back to the original object categories of the source dataset.

4. Experiments

Datasets. There are two VIS datasets with pixel-wise annotations: YouTube-VIS series [41] and OVIS [29]. For YouTube-VIS [41], we use the updated 2021 version (YTVIS21) in this paper. YTVIS21 contains 2,985 training, 421 validation, and 453 test videos over 40 categories. All the videos are annotated for every 5 frames. The number of frames per video is between 19 and 36. OVIS [29] includes 607 training, 140 validation and 154 test videos, scoping

L_{proj}	L_{pair}	$L_{pse\text{-}mask}$	YTVIS21	OVIS
✓			36.7	18.7
✓	✓		39.3	22.1
✓	✓	0.5	40.5	23.3
✓	✓	ϵ	41.2	23.9

Table 3. Ablation studies on BoxVIS baseline trained on YTVIS21 or OVIS, where ‘ ϵ ’ refers to the dynamic threshold for selecting high-quality pseudo masks.

25 object categories. Different from YTVIS21, videos in OVIS are longer (up to 292 frames) and have more objects with different occlusion levels per frame.

Our proposed BVISD with only box annotations contains 3524 videos from the above two VIS benchmarks and around 90k short pseudo video clips converted from COCO in the training set, and 362 videos in the validation set. BVISD combines all video types in both YTVIS21 and OVIS, and consists of 40 object categories.

Evaluation metrics. The metrics, including average precision (AP_*) at different IoU thresholds, average recall (AR_*) with different object numbers and the mean value of AP (AP), are adopted for VIS model evaluation. OVIS divides instances into three groups called slightly occluded (AP_{so}), moderately occluded (AP_{mo}) and heavily occluded (AP_{ho}) ones, whose occlusion scores are in the range of [0, 0.25], [0.25, 0.5] and [0.5, 0.75], respectively.

Implementation details. Unless otherwise stated, we employ the same hyper-parameters as Mask2Former-VIS [7], which is implemented on top of detectron2 [40]. All VIS models has been pre-trained on COCO image instance segmentation [24] with pixel-wise annotations.

The initial learning rate is set to 0.0001, and it decays by a factor of 0.1 at 10k and 12k iterations. The batch size adopts 16 video clips, and each video clip consists of 3 frames. During training, we resize the video clips with their shorter edge size being 320 and 512, and keep their longer edge size below 800. During inference, all frames are resized to a shorter edge size of 360 on YTVIS21 and 480 on OVIS and BVISD. We employ the tracking by query matching method proposed in [15] to associate the instances across clips, and adopt the average of its predicted masks in the overlapping clips as the final masks.

4.1. Ablation study

Losses in BoxVIS baseline (M2F-VIS-box). We study the effectiveness of the two box-supervised segmentation loss items and pseudo-mask loss in Table 3. One can see that BoxVIS baseline trained with only the projection loss L_{proj} performs poorly, while the introduction of the pairwise affinity loss L_{pair} improves the performance by 2.6% and 3.4% AP on YTVIS21 and OVIS, respectively. After applying the pseudo-mask loss $L_{pse\text{-}mask}$ with the high-

$ E_s $	$ E_t $	S_{lab}	S_{corr}	Shifting	YTVIS21	OVIS	BVISD
2		✓			41.1	25.5	31.9
2	3	✓			41.9	26.2	32.6
2	3	✓	✓		42.3	25.0	33.3
2	3	✓	✓	✓	42.6	26.5	33.8
2	5	✓	✓	✓	43.0	26.9	34.0

Table 4. Ablation studies on the STPA loss, where $|\cdot|$ denotes the number of pixels in the set.

Training data			Inference data		
YTVIS21	OVIS	COCO	YTVIS21	OVIS	BVISD
1			42.8	-	-
	1		-	26.2	-
1/2	1/2		41.5	27.0	32.7
2/3	1/3		42.3	27.9	34.2
1/2	1/4	1/4	43.2	29.0	35.5

Table 5. Ablation study on BVISD with different sampling weights during training.

quality pseudo masks, the performance can be further improved to 41.2% and 23.9% AP on YTVIS21 and OVIS, respectively, which is comparable to its pixel-supervised counterpart M2F-VIS shown in Table 1. The use of dynamic threshold for selecting high-quality pseudo masks brings another 0.7% AP increase in performance.

Components of the STPA loss. In Table 4, we explore the effects of the spatial-temporally paired pixels E_s and E_t , the patch correlation S_{corr} , and box-center guided shifting in the proposed STPA loss. We only adopt the box-supervised loss and exclude the pseudo-mask loss to better investigate the performance changes.

The pairwise affinity loss L_{pair} employs the spatially paired pixels E_s and the color similarity S_{lab} , obtaining 41.1%, 25.5% and 31.9% AP on YTVIS21, OVIS and BVISD datasets, respectively. Introducing the temporally paired pixels E_t into the STPA loss brings 0.7-0.9% AP improvements on all VIS datasets. However, if we directly add the patch correlation S_{corr} to the pairwise affinity, the performance only improves slightly on YTVIS21 and BVISD, while drops significantly on OVIS. This is because videos in OVIS have many crowded and similar-looking instances, and two patches with high correlation may come from different objects, resulting in incorrect pixel-wise supervision. Fortunately, by introducing the box-center guided shifting, this issue can be alleviated and the STPA loss achieves good performance on all VIS datasets. In addition, increasing the number of temporally paired pixels $|E_t|$ can slightly increase the performance. Overall, compared with the pairwise affinity loss used in IIS task, our specially designed STPA loss for VIS task can bring approximately 2% AP improvement on all VIS datasets.

Sampling weights in BVISD. Due to the unbalanced

Method	Training data	YTVIS21					OVIS					FPS	Params
		AP	AP ₅₀	AP ₇₅	AR ₁	AR ₁₀	AP	AP ₅₀	AP ₇₅	AR ₁	AR ₁₀		
<i>Pixel-wise annotations</i>													
CrossVIS [42]	YTVIS21 / OVIS	33.3	53.8	37.0	30.1	37.6	14.9	32.7	12.1	10.3	19.8	39.8	37.5M
VisTR [36]	YTVIS21 / OVIS	31.8	51.7	34.5	29.7	36.9	10.2	25.7	7.7	7.0	17.4	30.0	57.2M
IFC [16]	YTVIS21 / OVIS	36.6	57.9	39.3	-	-	13.1	27.8	11.6	9.4	23.9	46.5	39.3M
SeqFormer [37]	YTVIS21 / OVIS	40.5	62.4	43.7	36.1	48.1	15.1	31.9	13.8	10.4	27.1	72.3	49.3M
IDOL [38]	YTVIS21 / OVIS	43.9	68.0	49.6	38.0	50.9	24.3	<u>45.1</u>	23.3	<u>14.1</u>	33.2	30.6	43.1M
M2F-VIS [7]	YTVIS21 / OVIS	43.1	63.3	46.2	39.1	51.0	24.5	44.6	<u>23.6</u>	12.8	29.2	68.8	44.0M
MinVIS [15]	YTVIS21 / OVIS	44.2	66.0	48.1	<u>39.2</u>	<u>51.7</u>	26.3	47.9	25.1	14.6	<u>30.0</u>	52.4	44.0M
VITA [14]	YTVIS21 / OVIS	45.7	67.4	<u>49.5</u>	40.9	53.6	19.6	41.2	17.4	11.7	26.0	33.7	57.2M
<i>Box annotations</i>													
M2F-VIS-box	YTVIS21 / OVIS	41.2	63.3	44.6	37.9	48.5	23.9	46.5	22.8	13.6	28.1	37.8	44.0M
BoxVIS (our)	YTVIS21 / OVIS	42.8	64.9	47.3	38.0	49.3	26.2	49.4	26.3	13.6	30.0	37.8	44.0M
BoxVIS (our)	BVISD	43.2	66.8	46.6	39.0	50.7	29.0	52.2	29.1	14.8	33.1	37.8	44.0M

Table 6. Quantitative performance comparison of pixel-supervised and box-supervised VIS methods with ResNet50 backbone on YTVIS21 and OVIS, where FPS is computed on YTVIS21 valid set. Best in **bold**, and second best with underline.

number of objects per category in BVISD (see Fig. 2), we propose to sample the video clips from the three datasets with different sampling weights during training. Taking the last row of Table 5 as an example, among the 8 short video clips, 4, 2 and 2 are from YTVIS21, OVIS and COCO, respectively. BoxVIS trained separately on YTVIS21 or OVIS obtains 42.8% and 26.2% AP, respectively, while the model trained jointly on YTVIS21 and OVIS with equal sampling weights shows a performance drop on YTVIS21 but a slight performance increase on OVIS. This is because some object categories present in YTVIS21 are not in OVIS. By setting a higher sampling weight on YTVIS21, the performance is much improved on all VIS datasets. By using the pseudo video clips from COCO, BoxVIS can achieve about 1% AP improvement on all VIS datasets, verifying the values of our BVISD. Unless specified, the sampling weights in BVISD are set as 1/2, 1/4 and 1/4 for YTVIS21, OVIS and COCO data, respectively.

4.2. Main results

With ResNet50 backbones and Swin Large backbone, we compare the proposed BoxVIS with the state-of-the-art pixel-supervised VIS methods on YTVIS21 and OVIS datasets in Table 6 and Table 7, respectively.

YTVIS21 valid set. From Table 6, we can see that the performance of early pixel-supervised VIS methods [16, 36, 37, 42] is below 41% AP, mainly because the segmentation heads and tracking strategies are not well explored. The recently developed pixel-supervised VIS methods with self-supervised learning or masked-attention transformer bring nearly 4% and 5% AP improvement. Trained jointly on VIS and COCO datasets, VITA [14] achieves 45.7% AP by taking the whole video as input. Our proposed BoxVIS baseline, *i.e.*, M2F-VIS-box, obtains 41.2% AP,

1.9% and 4.5% AP lower than its pixel-supervised counterpart M2F-VIS [7] and the state-of-the-art VITA [14]. In contrast, our BoxVIS with the STPA loss can increase the performance to 42.8% AP, and our BoxVIS trained on BVISD improves the performance to 43.2% AP. Overall, our BoxVIS outperforms its pixel-supervised counterpart M2F-VIS [7] and exhibits comparable performance to the state-of-the-art pixel-supervised competitors.

OVIS valid set. In Table 6, the early proposed pixel-supervised VIS methods fail to handle the challenging videos in OVIS dataset, resulting in poor performance (below 15% AP). The latest masked-attention based methods M2F-VIS [7] and MinVIS [15] bring approximately 10% AP improvement, achieving 24.5% and 26.3% AP, respectively. However, VITA [14], which is the state-of-the-art on YTVIS21, obtains only 19.6% AP on OVIS, showing limited model generalization capability. The box-supervised baseline M2F-VIS-box and our BoxVIS trained only on OVIS obtain 23.9% and 26.2% AP, respectively, validating that the proposed STPA loss can predict instance masks with better spatial and temporal consistency. Finally, our BoxVIS trained on BVISD can improve the performance to 29.0% AP, even outperforming the state-of-the-art pixel-supervised VIS competitors. The encouraging results demonstrate the good generalization capability and great potentials of box annotation in VIS tasks.

Swin Large backbone. VIS models with the stronger Swin Large backbone can have higher detection and segmentation abilities. Due to the limited space, only the recently proposed high-performance methods are reported in Table 7. Among the pixel-supervised VIS methods, VITA [14] shows the best accuracy (57.5% AP) on YTVIS21, while MinVIS [15] and IDOL achieve 41.6% and 42.6% AP by taking 480p and 720p videos as input, respectively.

Method	Super.	AP	AP ₅₀	AP ₇₅	AR ₁	AR ₁₀
SeqFormer [37]	Pixel	51.8	74.6	58.2	42.8	58.1
IDOL [38]	Pixel	56.1	80.8	63.5	45.0	60.1
MinVIS [15]	Pixel	55.3	76.6	62.0	45.9	60.8
M2F-VIS [7]	pixel	52.6	76.4	57.2	-	-
VITA [14]	Pixel	57.5	80.6	61.0	47.7	62.6
BoxVIS	Box	52.8	75.4	58.3	44.4	58.1

(a) Performance comparison on YTVIS21

Table 7. Quantitative performance comparison of pixel-supervised and box-supervised VIS methods with Swin Large (SwinL) backbone [32] on YTVIS21 and OVIS respectively. Symbol ‘†’ means that the input video is of 720p.

Method	Super.	AP	AP ₅₀	AP ₇₅	AP _{so}	AP _{mo}	AP _{ho}
MinVIS [15]	Pixel	41.6	65.4	43.4	65.5	48.5	20.5
M2F-VIS [7]	pixel	26.4	50.2	26.9	46.1	30.9	9.5
VITA [14]	Pixel	27.7	51.9	24.9	-	-	-
IDOL † [38]	Pixel	42.6	65.7	45.2	-	-	-
BoxVIS	Box	34.4	59.0	33.8	56.8	39.5	14.6

(b) Performance comparison on OVIS



Figure 3. Box-supervised instance segmentation on two challenging videos in OVIS valid set. The first row shows the results of crowded objects with heavy occlusion, while the second row shows the results of two objects with complex boundary.

Our BoxVIS achieves 52.8% and 34.4% AP on YTVIS21 and OVIS, respectively, outperforming its pixel-supervised counterpart M2F-VIS [7]. With the Swin Large backbone, there is a performance gap between the pixel-supervised and box-supervised VIS methods. We believe one reason is that the transformer backbone can learn more priors than the CNN backbone from the pixel-wise annotation. Nonetheless, it should be noted that our BVISD consumes only 16% the cost of pixel-wise annotation, and there is a big room for BoxVIS to improve its performance.

Visualization. Fig. 3 displays the predicted instance masks by BoxVIS on two challenging videos in OVIS valid set. One can see that with only box annotations, BoxVIS trained on BVISD can still predict high-quality instance masks for challenging videos with occluded objects and complex boundaries. Visualization comparison on more videos are provided in the **supplemental materials**.

Parameters and Speed. We follow Detectron2 [40] to calculate the number of parameters and FPS for all VIS methods in Table 6. BoxVIS inherits the network architecture of M2F-VIS [7] and thus has the same model size (44M) as it. The tracking strategy affects mostly the inference speed of VIS models. SeqFormer [37] and M2F-VIS [7] take the whole video as input without extra track-

ing, running at around 70FPS. IDOL [38] and MinVIS [15] with frame-by-frame online inference run at 30.6FPS and 52.4FPS, respectively. Our BoxVIS adopts clip-by-clip near-online inference to obtain averaged masks on the overlapping clips, resulting in a slower inference speed at 37.8FPS. If we set the clip length as 1, BoxVIS can run as fast as M2F-VIS (*i.e.*, 70FPS) at the price of slight drop (about 1% AP on all VIS datasets).

5. Conclusion

This paper explored the feasibility of using only box annotations for VIS. We first extended the pixel-supervised VIS methods to a box-supervised VIS (BoxVIS) baseline, and proposed a spatial-temporal pairwise affinity (STPA) loss to introduce temporal pixel-wise mask supervision. Finally, we collected a large scale box-supervised VIS dataset (BVISD). The experimental results showed that with the ResNet50 backbone, the proposed BoxVIS trained on BVISD can yield high-quality object masks with decent spatial and temporal consistency, achieving comparable or even better performance than pixel-supervised VIS methods on YTVIS21 and OVIS. It is a promising direction to further investigate more effective BoxVIS models.

References

- [1] Ali Athar, Sabarinath Mahadevan, Aljoša Ošep, Laura Leal-Taixé, and Bastian Leibe. Stem-seg: Spatio-temporal embeddings for instance segmentation in videos. In *Eur. Conf. Comput. Vis.*, 2020. 2
- [2] Gedas Bertasius and Lorenzo Torresani. Classifying, segmenting, and tracking object instances in video with mask propagation. In *IEEE Conf. Comput. Vis. Pattern Recog.*, pages 9739–9748, 2020. 2
- [3] Daniel Bolya, Chong Zhou, Fanyi Xiao, and Yong Jae Lee. Yolact: Real-time instance segmentation. In *Int. Conf. Comput. Vis.*, pages 9157–9166, 2019. 2
- [4] Jiale Cao, Rao Muhammad Anwer, Hisham Cholakkal, Fahad Shahbaz Khan, Yanwei Pang, and Ling Shao. SipMask: Spatial information preservation for fast image and video instance segmentation. *arXiv preprint arXiv:2007.14772*, 2020. 2
- [5] Nicolas Carion, Francisco Massa, Gabriel Synnaeve, Nicolas Usunier, Alexander Kirillov, and Sergey Zagoruyko. End-to-end object detection with transformers. In *Eur. Conf. Comput. Vis.*, pages 213–229. Springer, 2020. 2
- [6] Ting Chen, Simon Kornblith, Mohammad Norouzi, and Geoffrey Hinton. A simple framework for contrastive learning of visual representations. pages 1597–1607. PMLR, 2020. 2
- [7] Bowen Cheng, Anwesa Choudhuri, Ishan Misra, Alexander Kirillov, Rohit Girdhar, and Alexander G Schwing. Mask2former for video instance segmentation. *arXiv preprint arXiv:2112.10764*, 2021. 1, 2, 3, 4, 6, 7, 8, 11
- [8] Bowen Cheng, Ishan Misra, Alexander G. Schwing, Alexander Kirillov, and Rohit Girdhar. Masked-attention mask transformer for universal image segmentation. 2022. 2
- [9] Tianheng Cheng, Xinggang Wang, Shaoyu Chen, Qian Zhang, and Wenyu Liu. Boxteacher: Exploring high-quality pseudo labels for weakly supervised instance segmentation. *arXiv preprint arXiv:2210.05174*, 2022. 1, 3
- [10] Jifeng Dai, Haozhi Qi, Yuwen Xiong, Yi Li, Guodong Zhang, Han Hu, and Yichen Wei. Deformable convolutional networks. In *Int. Conf. Comput. Vis.*, pages 764–773, 2017. 2
- [11] Lee R Dice. Measures of the amount of ecologic association between species. *Ecology*, 26(3):297–302, 1945. 4
- [12] Yuxin Fang, Shusheng Yang, Xinggang Wang, Yu Li, Chen Fang, Ying Shan, Bin Feng, and Wenyu Liu. Instances as queries. *arXiv preprint arXiv:2105.01928*, 2021. 2
- [13] Kaiming He, Georgia Gkioxari, Piotr Dollár, and Ross Girshick. Mask R-CNN. In *Int. Conf. Comput. Vis.*, pages 2961–2969, 2017. 2
- [14] Miran Heo, Sukjun Hwang, Seoung Wug Oh, Joon-Young Lee, and Seon Joo Kim. Vita: Video instance segmentation via object token association. 2022. 1, 2, 7, 8
- [15] De-An Huang, Zhiding Yu, and Anima Anandkumar. Min-vis: A minimal video instance segmentation framework without video-based training. *Adv. Neural Inform. Process. Syst.*, 2022. 1, 2, 6, 7, 8
- [16] Sukjun Hwang, Miran Heo, Seoung Wug Oh, and Seon Joo Kim. Video instance segmentation using inter-frame communication transformers. *Adv. Neural Inform. Process. Syst.*, 34:13352–13363, 2021. 1, 2, 7
- [17] Lei Ke, Xia Li, Martin Danelljan, Yu-Wing Tai, Chi-Keung Tang, and Fisher Yu. Prototypical cross-attention networks for multiple object tracking and segmentation. *Adv. Neural Inform. Process. Syst.*, 34:1192–1203, 2021. 2
- [18] Prannay Khosla, Piotr Teterwak, Chen Wang, Aaron Sarna, Yonglong Tian, Phillip Isola, Aaron Maschinot, Ce Liu, and Dilip Krishnan. Supervised contrastive learning. *Adv. Neural Inform. Process. Syst.*, 33:18661–18673, 2020. 2
- [19] Shiyi Lan, Xitong Yang, Zhiding Yu, Zuxuan Wu, Jose M Alvarez, and Anima Anandkumar. Vision transformers are good mask auto-labelers. *arXiv preprint arXiv:2301.03992*, 2023. 1
- [20] Shiyi Lan, Zhiding Yu, Christopher Choy, Subhashree Radhakrishnan, Guilin Liu, Yuke Zhu, Larry S Davis, and Anima Anandkumar. Discobox: Weakly supervised instance segmentation and semantic correspondence from box supervision. In *Int. Conf. Comput. Vis.*, pages 3406–3416, 2021. 1, 3
- [21] Minghan Li, Shuai Li, Lida Li, and Lei Zhang. Spatial feature calibration and temporal fusion for effective one-stage video instance segmentation. In *IEEE Conf. Comput. Vis. Pattern Recog.*, pages 11215–11224, 2021. 2
- [22] Wentong Li, Wenyu Liu, Jianke Zhu, Miaomiao Cui, Xian-Sheng Hua, and Lei Zhang. Box-supervised instance segmentation with level set evolution. In *Eur. Conf. Comput. Vis.*, pages 1–18. Springer, 2022. 1, 3
- [23] Huaijia Lin, Ruizheng Wu, Shu Liu, Jiangbo Lu, and Jiaya Jia. Video instance segmentation with a propose-reduce paradigm. *arXiv preprint arXiv:2103.13746*, 2021. 2
- [24] Tsung-Yi Lin, Michael Maire, Serge Belongie, James Hays, Pietro Perona, Deva Ramanan, Piotr Dollár, and C Lawrence Zitnick. Microsoft COCO: Common objects in context. In *Eur. Conf. Comput. Vis.*, pages 740–755. Springer, 2014. 1, 5, 6
- [25] Dongfang Liu, Yiming Cui, Wenbo Tan, and Yingjie Chen. Sg-net: Spatial granularity network for one-stage video instance segmentation. In *IEEE Conf. Comput. Vis. Pattern Recog.*, pages 9816–9825, 2021. 2
- [26] Fausto Milletari, Nassir Navab, and Seyed-Ahmad Ahmadi. V-net: Fully convolutional neural networks for volumetric medical image segmentation. In *2016 fourth international conference on 3D vision (3DV)*, pages 565–571. Ieee, 2016. 4
- [27] Jiangmiao Pang, Linlu Qiu, Xia Li, Haofeng Chen, Qi Li, Trevor Darrell, and Fisher Yu. Quasi-dense similarity learning for multiple object tracking. In *IEEE Conf. Comput. Vis. Pattern Recog.*, pages 164–173, 2021. 2
- [28] Dim P Papadopoulos, Jasper RR Uijlings, Frank Keller, and Vittorio Ferrari. Extreme clicking for efficient object annotation. In *Int. Conf. Comput. Vis.*, pages 4930–4939, 2017. 1, 5
- [29] Jiyang Qi, Yan Gao, Yao Hu, Xinggang Wang, Xiaoyu Liu, Xiang Bai, Serge Belongie, Alan Yuille, Philip Torr, and Song Bai. Occluded video instance segmentation: Dataset and challenge. In *Thirty-fifth Conference on Neural Infor*

mation Processing Systems Datasets and Benchmarks Track, 2021. 1, 2, 5

- [30] Zhi Tian, Chunhua Shen, and Hao Chen. Conditional convolutions for instance segmentation. *arXiv preprint arXiv:2003.05664*, 2020. 2
- [31] Zhi Tian, Chunhua Shen, Xinlong Wang, and Hao Chen. BoxInst: High-performance instance segmentation with box annotations. In *IEEE Conf. Comput. Vis. Pattern Recog.*, 2021. 1, 2, 3
- [32] Ashish Vaswani, Noam Shazeer, Niki Parmar, Jakob Uszkoreit, Llion Jones, Aidan N Gomez, Łukasz Kaiser, and Illia Polosukhin. Attention is all you need. In *Adv. Neural Inform. Process. Syst.*, pages 5998–6008, 2017. 8
- [33] Tao Wang, Ning Xu, Kean Chen, and Weiyao Lin. End-to-end video instance segmentation via spatial-temporal graph neural networks. In *Int. Conf. Comput. Vis.*, pages 10797–10806, 2021. 2
- [34] Xinggang Wang, Jiapei Feng, Bin Hu, Qi Ding, Longjin Ran, Xiaoxin Chen, and Wenyu Liu. Weakly-supervised instance segmentation via class-agnostic learning with salient images. In *IEEE Conf. Comput. Vis. Pattern Recog.*, pages 10225–10235, 2021. 2
- [35] Xinlong Wang, Rufeng Zhang, Chunhua Shen, Tao Kong, and Lei Li. Dense contrastive learning for self-supervised visual pre-training. In *IEEE Conf. Comput. Vis. Pattern Recog.*, pages 3024–3033, 2021. 2
- [36] Yuqing Wang, Zhaoliang Xu, Xinlong Wang, Chunhua Shen, Baoshan Cheng, Hao Shen, and Huaxia Xia. End-to-end video instance segmentation with transformers. In *IEEE Conf. Comput. Vis. Pattern Recog.*, 2021. 1, 2, 7
- [37] Junfeng Wu, Yi Jiang, Song Bai, Wenqing Zhang, and Xiang Bai. Seqformer: Sequential transformer for video instance segmentation. In *Eur. Conf. Comput. Vis.*, 2022. 1, 2, 7, 8
- [38] Junfeng Wu, Qihao Liu, Yi Jiang, Song Bai, Alan Yuille, and Xiang Bai. In defense of online models for video instance segmentation. In *Eur. Conf. Comput. Vis.*, 2022. 1, 2, 7, 8
- [39] Jialian Wu, Sudhir Yarram, Hui Liang, Tian Lan, Junsong Yuan, Jayan Eledath, and Gerard Medioni. Efficient video instance segmentation via tracklet query and proposal. In *IEEE Conf. Comput. Vis. Pattern Recog.*, pages 959–968, 2022. 2
- [40] Yuxin Wu, Alexander Kirillov, Francisco Massa, Wan-Yen Lo, and Ross Girshick. Detectron2. <https://github.com/facebookresearch/detectron2>, 2019. 6, 8
- [41] Linjie Yang, Yuchen Fan, and Ning Xu. Video instance segmentation. In *Int. Conf. Comput. Vis.*, pages 5188–5197, 2019. 1, 2, 5
- [42] Shusheng Yang, Yuxin Fang, Xinggang Wang, Yu Li, Chen Fang, Ying Shan, Bin Feng, and Wenyu Liu. Crossover learning for fast online video instance segmentation. In *Int. Conf. Comput. Vis.*, pages 8043–8052, 2021. 2, 7

Supplementary Materials

In this supplementary file, we provide the following materials:

- More visual comparison of pixel-supervised and box-supervised VIS methods (*cf.* Section 4.2 in the main paper);
- More visualization of instance masks predicted by BoxVIS (*cf.* Section 4.2 in the main paper).

A. More visual comparison of pixel-supervised and box-supervised VIS methods

In Figs. 1 - 3, we provide more visual comparison results of instance masks predicted by M2F-VIS [7], M2F-VIS-box and our BoxVIS on videos with crowded scenes, blurred or occluded objects. It can be seen that compared to the box-supervised baseline M2F-VIS-box, our BoxVIS can predict instance masks with better spatial and temporal consistency. On the other hand, BoxVIS can yield instance masks of the same high quality as the pixel-supervised M2F-VIS [7].

B. Visualization of instance masks predicted by BoxVIS

In Fig. 7 and Fig. 8, we visualize instance masks predicted by BoxVIS on various videos of YTVIS21 and OVIS, demonstrating the model generalization ability.



Figure 4. Visual comparison of instance segmentation results by M2F-VIS (top), M2F-VIS-box (middle row) and BoxVIS (bottom row) on videos with crowded scenes.

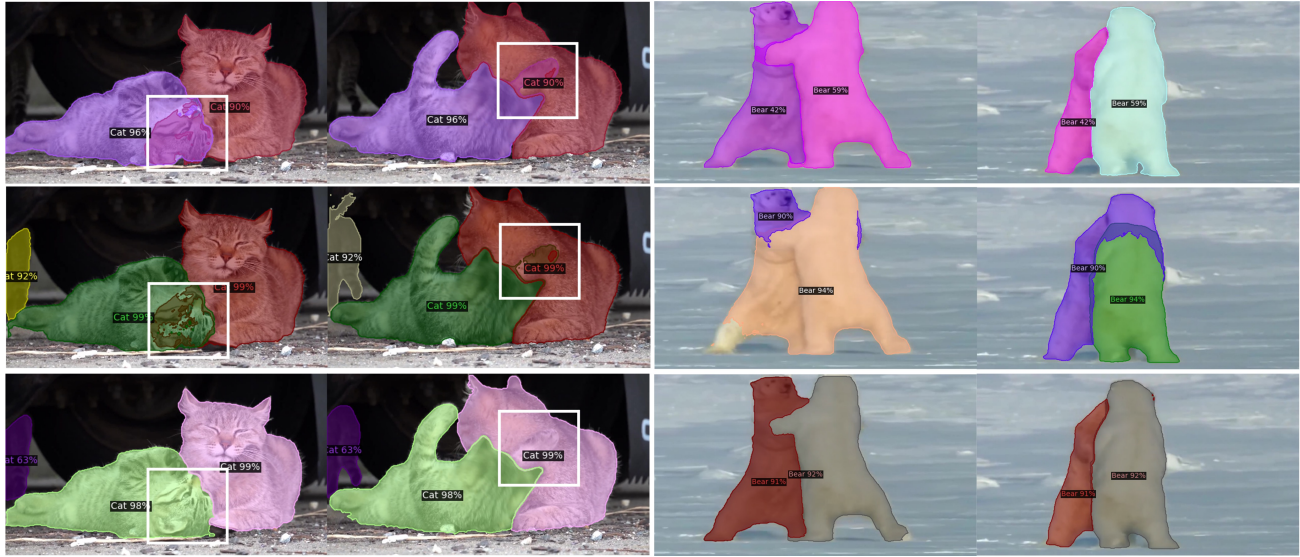


Figure 5. Visual comparison of instance segmentation results by M2F-VIS (top), M2F-VIS-box (middle row) and BoxVIS (bottom row) on videos with occluded objects.

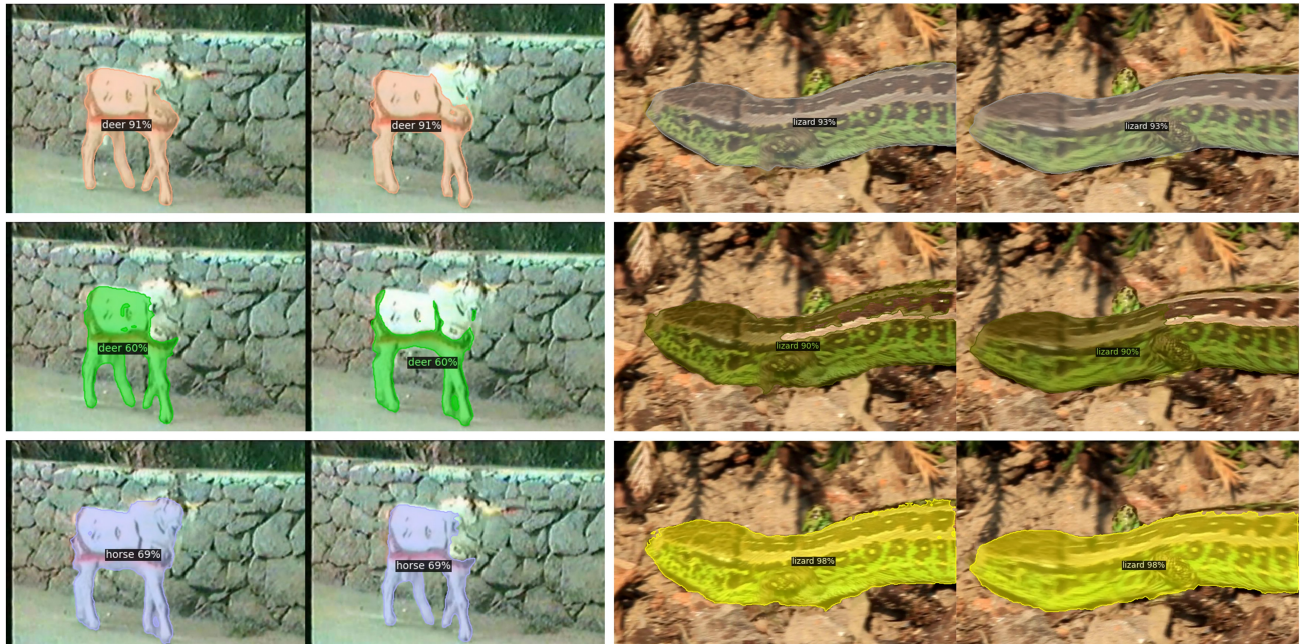


Figure 6. Visual comparison of instance segmentation results by M2F-VIS (top), M2F-VIS-box (middle row) and BoxVIS (bottom row) on videos with blurred objects.



Figure 7. Visualization of instance masks predicted by BoxVIS on YTVIS21 valid set.

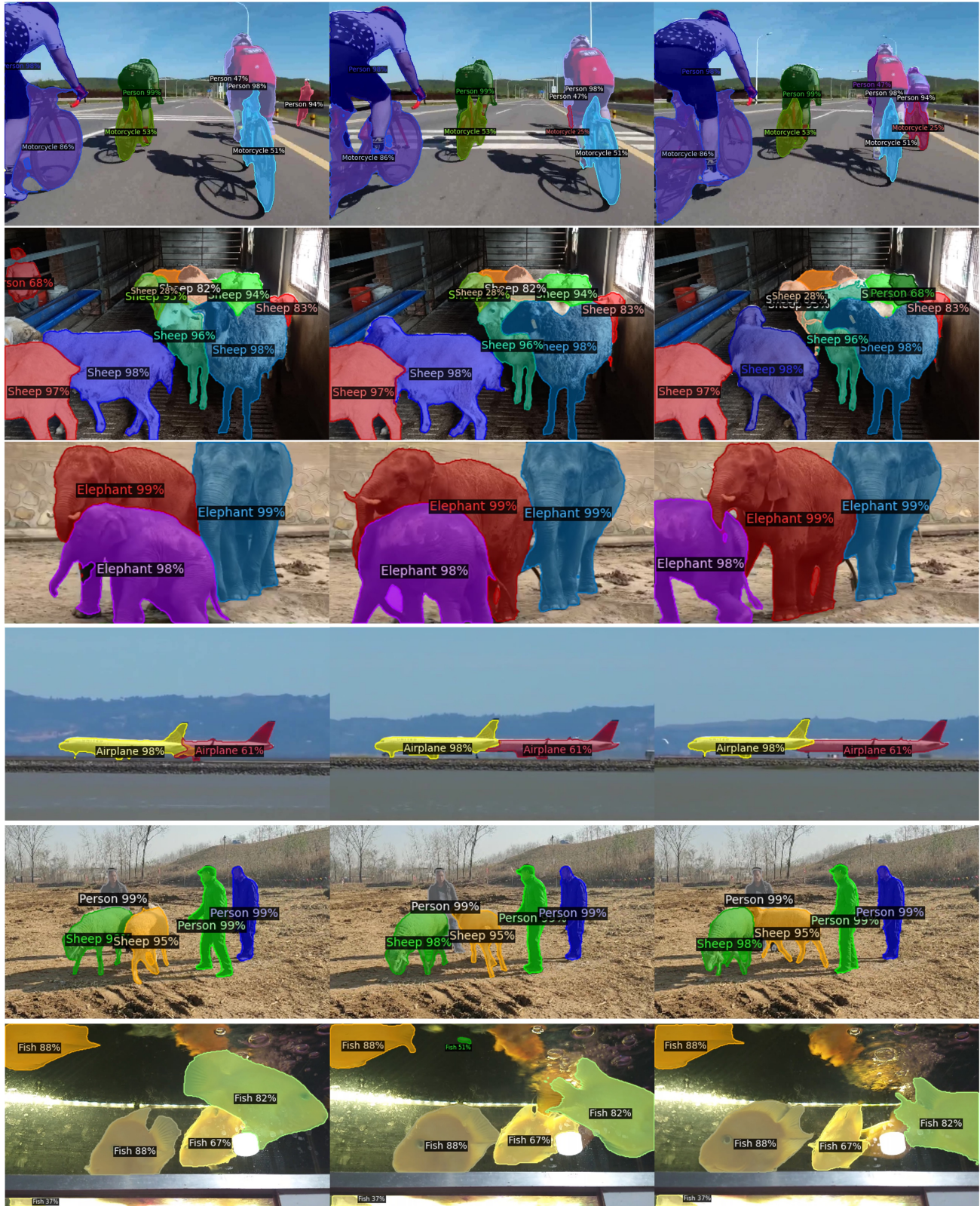


Figure 8. Visualization of instance masks predicted by BoxVIS on OVIS valid set.